Applied Mathematical Modelling 33 (2009) 3245–3257

Contents lists available at ScienceDirect

Applied Mathematical Modelling

journal homepage: www.elsevier.com/locate/apm

Green's function, temperature in a convectively cooled sphere with arbitrarily located spherical heat sources

Ayhan Yilmazer *

Department of Nuclear Engineering, Hacettepe University, 06800 Beytepe, Ankara, Turkey

ARTICLE INFO

Article history:
Received 3 July 2008
Received in revised form 17 October 2008
Accepted 22 October 2008
Available online 30 October 2008

Keywords:
Heat conduction
Robin boundary condition
Spherical harmonics
Pebble bed reactors
PBMR

ABSTRACT

Steady state heat conduction in a convectively cooled sphere having arbitrarily located spherical heat sources inside is treated with the method of Green's function accompanied by a coordinate transform. Green's function of the heat diffusion operator for a finite sphere with Robin boundary condition is obtained by spherical harmonics expansion. Verification of the analytical solution is exemplified in some generic cases related to the pebbles of South-African PBMR as of year 2000 with 268 MW thermal power. Analytical results for different sectors of the sphere (pebble) are compared with the results of computational fluid dynamics code FLUENT™. This work is motivated through a modest effort to assess the stochastic effects of distribution and volumetric effects of fuel kernels within the pebbles of future-promising pebble bed reactors.

1. Introduction

Green's function (GF) method is a conceptually elegant tool in the solution of linear differential equations describing a various range of physical problems such as diffusion, transport of particles, heat, etc. In the method, the diffusing (transporting) unknown quantity is given in an integral expression involving the boundary conditions and the GF. If the GF is known and the integral can be evaluated then the GF method is a powerful tool for solving a very wide range of problems. Evaluation of the integral is not an easy task in general and constitutes an integral part of the solution as will become apparent later in this work.

There is an extensive literature on the application of GF method. Cole and Yen [1] have provided a comprehensive literature on GF method: a good overview of the subject has been provided in classical books of Morse and Feshbach [2], Carlsaw and Jaeger [3] and Stakgold [4]. Barton [5] has carefully discussed the properties of the Dirac delta function and described pseudo GF for the Neumann boundary condition. Differential equations are organized using a number system according to the type of the differential equation in two books by Butkovskii [6,7]. A similar number system for the number of spatial dimensions, the order of the highest time derivative, and the order of the highest spatial derivative has been used by Beck et al. [8] to categorize Green's functions. Beck et al. [8] give extensive tables of GF for heat conduction and diffusion. The steady 2D heat conduction in Cartesian and cylindrical coordinates has been discussed by Dolgova and Melnikov [9]. Following Dolgova and Melnikov, the approach of identifying slowly converging portions of Fourier series expansion and replacing them with the closed form expressions has been extended and expanded in two recent books by Melnikov [10,11]. With this approach numerical convergence of the GF method has been improved for a variety of equations, coordinate systems and boundary conditions. The work on heat conduction in a rectangle by Cole and Kim [12] provides a complete list of all

* Tel.: +90 312 2977300; fax: +90 312 2992122.
E-mail addresses: yilmazer@hacettepe.edu.tr, yilmazer@nuke.hacettepe.edu.tr

0307-904X/$ - see front matter
doi:10.1016/j.apm.2008.10.025

Nomenclature

α	rotation (Euler) angle about z-axis
β	rotation (Euler) angle about y-axis
Bi	Biot number
D	pebble diameter
ε	void fraction
f_ε	arrangement factor
g_ℓ	radial part of Green's function
G	Green's function
h	convection coefficient
k	conduction coefficient
μ	dynamic viscosity
Δ	Laplacian operator
N	number of spherical sources
Nu	Nusselt number
$\mathbf{n}$	unit normal vector
P_ℓ	Legendre function of degree ℓ
P_ℓ^m	associated Legendre function of degree ℓ order m
Pr	Prandtl number
ϕ	azimuth angle
q	source strength
$\dot{q}$	volumetric heat generation rate
$\mathbf{r}$	position vector
R	pebble radius
R_i	source radius
S	surface
ψ	excess temperature
T	temperature
θ	zenith angle
V	coolant velocity, volume
Y_ℓ^m	spherical harmonics of degree ℓ order m

Subscripts

eff	effective
i	source index
∞	bulk coolant
l	laminar
s	single sphere
t	turbulent

single-sum GF with boundary conditions of type 1, 2, or 3. In their subsequent work, Cole and Yen [1] have replaced hyperbolic functions with a single-sum form involving exponentials and demonstrated better convergency.

Solution of heat conduction or other diffusion-like problems by GF method have been carried out mostly in Cartesian or cylindrical coordinates because of the similarity of a variety of real systems or components to these geometries. A lot of numerical work has been published on heat transfer in solid spheres, for fluidized beds, cracking processes, etc. [13–15]. For the case of spherical coordinates, fuel pebbles of a pebble bed reactor, among promising candidates of generation IV nuclear reactors, would be a delightful application of the GF method due to the following reasons: spherical heat generating fuel kernels dispersed throughout the spherical pebble introduce an academically lively conduction problem. Additionally, typically limiting design criteria of maximum pebble temperature has been obtained for synthesized pebble bed or as a further step heat conduction equation is solved for a specified location of the reactor where gas and average pebble temperatures have already been calculated. When solving heat conduction equation in the pebble, heat generation of tiny spherical fuel particles (kernels) is assumed to be continuous throughout the pebble. However, solving the conduction equation for thousands of such kernels dispersed arbitrarily within the pebble is more realistic and would allow one to discuss stochastic effects of kernels' distribution on temperature and other dependent variables.

One of the crucial parameters effecting behavior of the fuel particles (kernels) is the temperature distribution within the pebble in which fuel particles are dispersed. Temperature field within the pebble has a major effect on the thermal stress distribution over the fuel particles and migration of fission products through coating layers of the fuel particle which may increase failure rate of fuel particles. Considering these facts, this work is motivated through a modest effort to assess the stochastic effects of distribution and volumetric effects of fuel kernels within the pebbles of future-promising pebble bed reactors. As an initiative step, it is aimed to investigate the feasibility of the GF method to the steady state heat conduction equation in a convectively cooled sphere having arbitrarily located spherical heat sources inside.

The paper is organized as follows: after a brief overview of the pebbles of a pebble bed reactor the heat diffusion problem in a sphere together with convective boundary conditions and effective physical properties are formulated. Following the formulation of GF solution of the problem, GF is obtained by using spherical harmonics expansion. Completing the analytical work, some generic cases are studied for the South-African pebble bed modular reactor (PBMR) with 268 MW thermal power [16]. Analytical results are compared with the computational fluid dynamics code FLUENT™. A brief conclusion is included particularly to explain the numerical difficulties encountered in the calculations.

2. Governing equations

Modern pebble bed reactor fuel elements are composed of small (0.5 mm diameter) uranium oxide (UO_2) kernels surrounded by various layers of prolific carbon, silicon carbide, and buffer graphite [17]. Kernels composed of uranium carbide (UC_2) or a mixture of UO_2 and UC_2 have also been designed and fabricated. The prolific carbon layers are applied in chemical vapor deposition process to form fuel particle of just under 1 mm diameter. The layers serve as pressure boundary and retention zone for fission products. Many thousands of these so-called TRISO particles are then mixed with graphite binder. The mixture is formed into sphere of about 5 cm in diameter. A 0.5 cm layer of pure graphite surrounds the fuel zone to form the 6 cm pebble.

2.1. Heat diffusion equation

Heat diffusion equation for a spherical pebble is given as follows:

$$\Delta T + \frac{\dot{q}}{k_{eff}} = 0, \tag{1}$$

$$-k_{eff}\frac{\partial T}{\partial n} = h(T - T_\infty) \text{ on the surface of the pebble}, \tag{2}$$

where k_{eff} denotes the effective thermal conductivity of pebble in which N spherical sources are embedded, Δ is the Laplacian operator in spherical polar coordinates, h is the convection coefficient, and T_∞ is the bulk coolant temperature. Effective thermal conductivity approximation instead of handling the pebble as a composite material is reasonable due to comparatively small volume fraction (less then 1%) of fuel kernels in the pebble. Estimation of k_{eff} of heterogeneous solids could be made by Maxwell's formula [18]. Maxwell's derivation was for electrical conductivity, but the same arguments apply for thermal conductivity. He showed that k_{eff} of a material made of spheres of conductivity k_1 embedded in a continuous solid phase with conductivity k_o for small volume fraction of ϕ is given as

$$\frac{k_{eff}}{k_o} = 1 + \frac{3\phi}{\left(\frac{k_1+2k_o}{k_1-k_o}\right) - \phi}. \tag{3}$$

If the excess temperature is defined as

$$\psi(r,\theta,\phi) = T(r,\theta,\phi) - T_\infty, \tag{4}$$

Eqs. (1) and (2) take the form

$$\Delta\psi + \frac{\dot{q}}{k_{eff}} = 0, \tag{5}$$

$$\frac{\partial\psi}{\partial n} + \frac{Bi}{R}\psi = 0 \text{ on the surface of the graphite sphere}, \tag{6}$$

where $Bi = \frac{hR}{k}$ is the Biot number and $\frac{\partial}{\partial n}$ stands for outward normal derivative.

Lets assume that N spherical sources are located arbitrarily in a graphite sphere (PBR fuel element) of radius R and denote ith source strength by $q_i(W)$, radius R_i and location by (r_i, ϕ_i, θ_i). Lets further assume that volumetric heat generation rate in each spherical source (kernel) is uniform and given by $\dot{q}_i = q_i/V_i$ where V_i is the volume of ith spherical source. Contribution of a this single source to the excess temperature could be calculated by the solution of the following equations:

$$\Delta\psi_i(r,\phi,\theta) + \frac{\dot{q}_i}{k_{eff}} = 0, \tag{7}$$

$$\frac{\partial\psi_i}{\partial n} + \frac{Bi}{R}\psi_i = 0 \quad \text{at} \quad r = R. \tag{8}$$

Notice that k_{eff} is the one that used for N spheres, not only for ith source. Summing up excess temperature of all sources results in

$$\sum_{i=1}^{N} \psi_i(r,\phi,\theta) = \psi(r,\phi,\theta) = T(r,\phi,\theta) - T_\infty, \tag{9}$$

by virtue of principle of superposition.

2.2. Green's function formulation

Solving Eqs. (7) and (8) suffices to find the solution of the original problem numerated by Eqs. (1) and (2). In the primed coordinate system, Eqs. (7) and (8) for ith spherical source of radius R_i is located at $(r'_i, \phi'_i, \theta'_i)$ become

$$\Delta\prime\psi_i(r',\phi',\theta') + \frac{\dot{q}_i(r',\phi',\theta')}{k_{eff}} = 0, \tag{10}$$

$$\frac{\partial\psi_i}{\partial n} + \frac{Bi}{R}\psi_i(r',\phi',\theta') = 0 \quad \text{at} \quad r' = R. \tag{11}$$

In the same coordinate system, Green's function satisfies the following equations:

$$\Delta' G(r',\phi',\theta'/r,\phi,\theta) + \delta(\mathbf{r}' - \mathbf{r}) = 0, \tag{12}$$

$$\frac{\partial G}{\partial n} + \frac{Bi}{R} G(r',\theta',\phi'/r,\theta,\phi) = 0 \quad \text{at} \quad r' = R. \tag{13}$$

for a unit impulse source located at $\mathbf{r}' = \mathbf{r}$ and denoted by three-dimensional Dirac's delta function $\delta(\mathbf{r}' - \mathbf{r})$ in polar spherical coordinates.

If both sides of Eq. (10) is multiplied by$G$ and Eq. (12) by ψ_i, and then resulting two equations are subtracted and integrated over the volume V' of the graphite sphere bounded by a surface S'

$$\psi_i(r,\phi,\theta) = \int_{S'} \left(G\frac{\partial\psi_i}{\partial n} - \psi_i \frac{\partial G}{\partial n} \right) dS' + \int_{V'} \frac{\dot{q}_i}{k} G dV', \tag{14}$$

is obtained for the excess temperature after using Green's Theorem. The surface integral vanishes due to boundary conditions. Then, excess temperature becomes

$$\psi_i(r,\theta,\phi) = \frac{1}{k_{eff}} \int_{V'} \dot{q}_i(r',\phi',\theta') G(r',\phi',\theta'/r,\phi,\theta) dV'. \tag{15}$$

3. Finding Green's function

Using the below spherical harmonics expansion for Green's function [19]

$$G(r',\phi',\theta'/r,\phi,\theta) = \sum_{\ell=0}^{\infty} \sum_{m=-\ell}^{\ell} g_\ell(r',r) Y_\ell^m(\theta',\phi') Y_\ell^{m*}(\theta,\phi), \tag{16}$$

reciprocity property of Green's function yields in

$$G(r,\phi,\theta/r',\phi',\theta') = \sum_{\ell=0}^{\infty} \sum_{m=-\ell}^{\ell} g_\ell(r,r') Y_\ell^m(\theta,\phi) Y_\ell^{m*}(\theta',\phi'). \tag{17}$$

Eqs. (12) and (13) for the unprimed or physical coordinate systems take the following form:

$$\Delta G(r,\phi,\theta/r',\phi',\theta') + \delta(\mathbf{r} - \mathbf{r}') = 0, \tag{18}$$

$$\frac{\partial G}{\partial n} + \frac{Bi}{R} G(r,\phi,\theta) = 0 \quad \text{at} \quad r = R. \tag{19}$$

Three-dimensional Dirac delta function in spherical coordinates is known to be as

$$\delta(\mathbf{r} - \mathbf{r}') = \frac{\delta(r - r')}{r^2} \sum_{\ell=0}^{\infty} \sum_{m=-\ell}^{\ell} Y_\ell^m(\theta,\phi) Y_\ell^{m*}(\theta',\phi'). \tag{20}$$

Inserting spherical harmonics expansions of$G$ and $\delta(\mathbf{r} - \mathbf{r}')$ given by Eqs. (17) and (20), respectively, into Eq. (18), following differential equation for the radial part of the Green's function is obtained:

$$r\frac{d^2}{dr^2}[r g_\ell(r,r')] - \ell(\ell+1) g_\ell(r,r') = -\delta(r - r'). \tag{21}$$

Independent solutions of the homogeneous form of the above equation are r^ℓ and $r^{-\ell-1}$. Therefore, $g_\ell(r,r')$ can be chosen as

$$g_\ell(r,r') = \begin{cases} g_\ell^1(r,r') = Ar^\ell + Br^{-\ell-1}; & r < r', \\ g_\ell^2(r,r') = Cr^\ell + Dr^{-\ell-1}; & r > r'. \end{cases} \tag{22}$$

Since $g_\ell(r,r')$ must be finite at $r = 0$, B vanishes. Continuity at $r = r'$ reads as

$$g_1(r,r') = g_2(r,r') \quad \text{at} \quad r = r'. \tag{23}$$

Integrating Eq. (21) in the neighborhood of $r = r'$ results in

$$\int_{r'-\varepsilon}^{r'+\varepsilon} \frac{d^2}{dr^2}[rg_\ell(r,r')]dr - \int_{r'-\varepsilon}^{r'+\varepsilon} \frac{\ell(\ell+1)g_\ell(r,r')}{r}dr = -\int_{r'-\varepsilon}^{r'+\varepsilon} \frac{\delta(r-r')}{r}dr. \tag{24}$$

In the limiting case, when $\varepsilon \to 0$ second integral on the left-hand side vanishes since $\frac{\ell(\ell+1)g_\ell(r,r')}{r}$ is continuous at $r = r'$, and right hand side becomes $\frac{1}{r'}$ due to the sifting property of the Dirac's Delta function. Then, jump discontinuity at $r = r'$ becomes

$$\frac{d}{dr}[rg_\ell^2(r,r')]_{r=r'} - \frac{d}{dr}[rg_\ell^1(r,r')]_{r=r'} = -\frac{1}{r'}. \tag{25}$$

GF takes the homogeneous form of the boundary condition on the surface; refer to Eq. (19), of the sphere as follows:

$$\frac{d}{dr}[g_\ell^2(r,r')]_{r=R} + \frac{Bi}{R}g_\ell^2(r,r')]_{r=R} = 0. \tag{26}$$

Using Eqs. (23), (25) and (26) the radial part of the Green's Function is obtained as follows:

$$g_\ell(r,r') = \begin{cases} g_\ell^1(r,r') = \left[\left(\frac{r'^\ell}{R^{2\ell+1}}\right)\left(\frac{\ell+1-Bi}{\ell+Bi}\right) + r'^{(-\ell-1)}\right]\frac{r^\ell}{2\ell+1}; & r < r', \\ g_\ell^2(r,r') = \left[\left(\frac{r^\ell}{R^{2\ell+1}}\right)\left(\frac{\ell+1-Bi}{\ell+Bi}\right) + r^{(-\ell-1)}\right]\frac{r'^\ell}{2\ell+1}; & r > r'. \end{cases} \tag{27}$$

4. Examples

In this part, our analytical solution is exemplified in some generic cases starting from the simplest to more general case. Verification for a single spherical source which is eccentric with the pebble is the simplest case and achieved easily. Calculated results for a single non-eccentric spherical source placed on a specified coordinate axis which corresponds to the azimuthally symmetric case are compared with the CFD code FLUENT. Comparison for a single spherical source placed arbitrarily within the pebble is made with FLUENT too. Similar runs and comparisons are carried out up to three spherical sources located within pebble. Since the kernels have diameters negligible in comparison with pebble diameter, volumetric effects is investigated by taking kernels as point sources in the calculations carried out for three sources.

The computational grids for all cases considered are generated using GAMBIT software. Tetrahedral meshes are used. To guarantee mesh size-independent results, various mesh sizes are tested. After 200,000 meshes no significant changes are observed in the calculated temperatures. Hence, 230,000 meshes are selected in the computations. In a computer with a 3.0 GHz-Pentium 4 processor, it takes approximately 2 min to obtain converged results.

Calculations, in all of the following case studies, are based on the data relevant to the South-African PBMR as of year 2000 with 268 MW thermal power whose thermal-hydraulics data is given in Table 1.

Power production of the pebble for which temperature distribution is calculated is assumed to be 268 MW/330,000 = 8.121×10^2 W which is the average power production per pebble in the core. Total volume of 15,000 kernels, each with a diameter of 0.5 mm, within the graphite pebble is 9.817×10^{-1} cm^3 and the volume of one pebble with a diameter of 6 cm is 113.097 cm^3. The volume fraction of kernels in the pebble is about 0.868%. To develop a methodology to examine the effect of distribution of 15,000 kernels in graphite matrix (pebble) on temperature distribution calculations are started from

Table 1
Thermal-hydraulics data of PBMR-268.

PBMR-268 characteristics	
Core power	268 MW
Core diameter (m)	3.5
Core height (m)	8.5
Number of pebbles-fuel/graphite	330,000/110,000
Pebble packing fraction	0.613
Number of kernels per pebble	15,000
Pebble diameter (cm)	6.0
Kernel diameter (mm)	0.5
He temperature (°C) – inlet/outlet	503/900
He flow rate (kg/s)	125.74
He inlet pressure (Mpa)	7.0

a single spherical source located arbitrarily and having total volume of fuel kernels. Then, calculations are continued by dividing this spherical source into equal volumes of two, three, etc. The radius of the single spherical source corresponding to total volume of the kernel is 6.165×10^{-1} cm, of two spherical sources are 4.893×10^{-1} cm, and three spherical sources are 4.275×10^{-1} cm, respectively.

Gnielinski correlation [20] is used for the average Nusselt number. It is based on the assumption that heat transfer of pebble beds can be related to that of a single sphere by an arrangement factor f_ε dependent on the void fraction ε

$$Nu = f_\varepsilon Nu_s, \tag{28}$$

with

$$f_\varepsilon = 1 + 1.5(1 - \varepsilon). \tag{29}$$

Nusselt number for a single sphere is given as follows:

$$Nu_s = 2 + \sqrt{Nu_l^2 + Nu_t^2}, \tag{30}$$

with the Nusselt number given for laminar flow by

$$Nu_l = 0.663\left(\frac{Re}{\varepsilon}\right)^{1/2} Pr^{1/3}, \tag{31}$$

the Nusselt number for turbulent flow given by

$$Nu_l = \frac{0.037\left(\frac{Re}{\varepsilon}\right)^{0.8} Pr}{1 + 2.443\left(\frac{Re}{\varepsilon}\right)^{-0.1}(Pr^{2/3} - 1)}, \tag{32}$$

and the Reynolds number given by

$$Re = \frac{VD}{\mu}, \tag{33}$$

where V is the average He velocity throughout the core, D is the pebble diameter, and μ is the dynamic viscosity of the helium.

Helium is assumed to be at an average temperature of the core inlet and outlet temperatures of about 700 °C. Since the pressure drop throughout the core is small in comparison with the operating pressure 7 MPa, helium properties are calculated at these values of temperature and pressure considering it as an ideal gas. Convective heat transfer coefficient h is taken as 4000 W/m^2 K in all of the subsequent calculations, an approximate value which is evaluated by using the Gnielinski correlation given by Eq. (28) and using thermal-hydraulics data of the reactor given in Table 1.

Effective conductivity of pebble depends on neutron irradiation and temperature. It is calculated at 700 °C by the following [21] empirical correlation:

$$k_{eff} = 1.2768\left[(-0.3906.T + 0.06829)/(DOSIS + 1.931.10^{-4}T + 0.105) + 1.228.10^{-4}.T + 0.042\right](\mathrm{W/m\ K}), \tag{34}$$

instead of using effective conductivity approximation of composite materials given by Eq. (3). T is in °C and$DOSIS$ stands for the fast neutron irradiation dose in Eq. (34). A value of 38 W/m K for effective conductivity is used in all calculations, which corresponds to zero irradiation rates (fresh fuel element).

4.1. Radially symmetric case

Let's assume a single spherical source of radius R_i with a uniform volumetric heat generation rate $\dot{q}_i$ is placed eccentrically with the graphite sphere of radius R. The problem could be stated as

$$\frac{1}{r^2}\frac{d}{dr}r^2\frac{d\psi_i(r)}{\partial r} + \frac{\dot{q}_i}{k_{eff}} = 0; \quad r \leqslant R_i, \tag{35}$$

$$\frac{1}{r^2}\frac{d}{dr}r^2\frac{d\psi_i(r)}{\partial r} = 0; \quad R_i \leqslant r \leqslant R, \tag{36}$$

$$\psi_i(R_i^-) = \psi_i(R_i^+), \tag{37}$$

$$-k_{eff}\frac{d\psi_i}{dr}\bigg|_{r=R^-} = -k_{eff}\frac{d\psi_i}{dr}\bigg|_{r=R^+}, \tag{38}$$

$$\frac{d\psi_i}{dr} + \frac{Bi}{R}\psi_i = 0 \quad \text{at} \quad r = R. \tag{39}$$

Analytical solution to the above set is simple and straightforward:

$$\psi_i(r) = T_i(r) - T_\infty = \frac{\dot{q}_i}{6k_{eff}}\left(R_i^2 - r^2\right) + \frac{\dot{q}_i R_i^3}{3R^2 h}\left[1 + \frac{hR^2}{k_{eff}}\left(\frac{1}{R_i} - \frac{1}{R}\right)\right]; \quad r \leqslant R_i, \tag{40}$$

$$\psi_i(r) = T_i(r) - T_\infty = \frac{\dot{q}_i R_i^3}{3R^2 h} + \frac{\dot{q}_i R_i^3}{3k_{eff}}\left(\frac{1}{r} - \frac{1}{R}\right); \quad R_i \leqslant r \leqslant R. \tag{41}$$

Let's prove that Green's function solution is identical to the solution given by Eqs. (40) and (41). Green's function solution given by Eq. (15) could be rearranged more explicitly as

$$\psi_i(r,\phi,\theta) = T_i(r,\phi,\theta) - T_\infty = \frac{1}{k_{eff}}\int_{r'=0}^{R}\int_{\theta'=0}^{\pi}\int_{\phi'=0}^{2\pi} G(r',\phi',\theta'/r,\phi,\theta)\dot{q}_i(r',\phi',\theta')\sin\theta' d\phi' d\theta' r'^2 dr'. \tag{42}$$

If spherical harmonics expansion of Green's function given by Eq. (17) is introduced into Eq. (42), excess temperature is obtained after using reciprocity property of Green's function as

$$\begin{aligned}\psi_i(r,\phi,\theta) = {} & \frac{\dot{q}_i}{k_{eff}}\int_{r'=0}^{r}\int_{\theta'=0}^{\pi}\int_{\phi'=0}^{2\pi}\sum_{\ell=0}^{\infty}\sum_{m=-\ell}^{\ell} g_\ell^2(r,r')Y_\ell^m(\theta,\phi)Y_\ell^{m*}(\theta',\phi')\sin\theta' d\phi' d\theta' r'^2 dr' \\ & + \frac{\dot{q}_i}{k_{eff}}\int_{r'=r}^{R}\int_{\theta'=0}^{\pi}\int_{\phi'=0}^{2\pi}\sum_{\ell=0}^{\infty}\sum_{m=-\ell}^{\ell} g_\ell^1(r,r')Y_\ell^m(\theta,\phi)Y_\ell^{m*}(\theta',\phi')\sin\theta' d\phi' d\theta' r'^2 dr'.\end{aligned} \tag{43}$$

Using

$$\int_0^{2\pi}\int_0^{\pi}\sin(\theta')Y_\ell^{m*}(\theta',\phi')d\theta' d\phi' = 2\sqrt{\pi}\delta_{\ell,0}\delta_{m,0}, \tag{44}$$

and

$$Y_0^0(\theta',\phi') = \frac{1}{2\sqrt{\pi}}. \tag{45}$$

Eq. (43) simplifies to

$$\psi_i(r,\phi,\theta) = \frac{\dot{q}_i}{k_{eff}}\left[\int_{r'=0}^{r} g_0^2(r,r')r'^2 dr' + \int_{r'=r}^{R_i} g_0^1(r,r')r'^2 dr'\right]; \quad 0 \leqslant r' = r \leqslant R_i \text{ (inside the source)}, \tag{46}$$

$$\psi_i(r,\phi,\theta) = \frac{\dot{q}_i}{k_{eff}}\int_{r'=0}^{R_i} g_0^2(r,r')r'^2 dr'; \quad R_i \leqslant r' = r \leqslant R \text{ (outside the source)}. \tag{47}$$

Green's function given by Eq. (27) for $\ell = 0$ becomes

$$g_0(r,r') = \begin{cases} g_0^1(r,r') = \left(\frac{1}{R}\right)\left(\frac{1-Bi}{Bi}\right) + r'^{-1}; & r < r', \\ g_0^2(r,r') = \left(\frac{1}{R}\right)\left(\frac{1-Bi}{Bi}\right) + r^{-1}; & r > r'. \end{cases} \tag{48}$$

Introducing Eq. (48) into Eqs. (46) and (47) and using the definition $Bi = hR/k_{eff}$ produce the same excess temperature distributions as Eqs. (40) and (41) which validates the GF solution for this simple case.

4.2. Azimuthally symmetric case

Let's consider a spherical source of radius R_i with a uniform volumetric heat generation rate $\dot{q}_i$, whose center is located on a specified axis, say z-axis, at a position $(0,0,z_i)$ within the graphite sphere of radius R (Fig. 1).

The main difficulty in the calculation of the temperature distribution within the pebble is to accomplish volume integration over the spherical source for different sectors of the computational domain which is the primed coordinate system in the Green's function solution given by (15). For this purpose graphite sphere of radius R is divided into three regions. *I* represents the sphere with a radius $z_i - R_i$ eccentric with the graphite sphere, *II* represents the spherical shell which extends from $r' = z_i - R_i$ to $r' = z_i + R_i$, and *III* is the outermost spherical shell beyond region *II* as shown in Fig. 1. Volume integration is carried out by a simple geometrical interpretation. The intersection of the sphere centered at the origin with radius r' and the spherical source with radius R_i centered at $(0,0,z_i)$ is the circle whose $y' - z'$ plane projection is shown by AB-line in Fig. 1. Equations representing these two spheres are

$$\begin{aligned} x'^2 + y'^2 + z'^2 &= r'^2 \\ x'^2 + y'^2 + (z'-z_i)^2 &= R_i^2 \end{aligned}; \quad R_i \leqslant r' = r \leqslant R. \tag{49}$$

Solving Eq. (49) together gives the equation of the AB-line as follows:

$$z' = \frac{z_i^2 - R_i^2 + r'^2}{2z_i}. \tag{50}$$

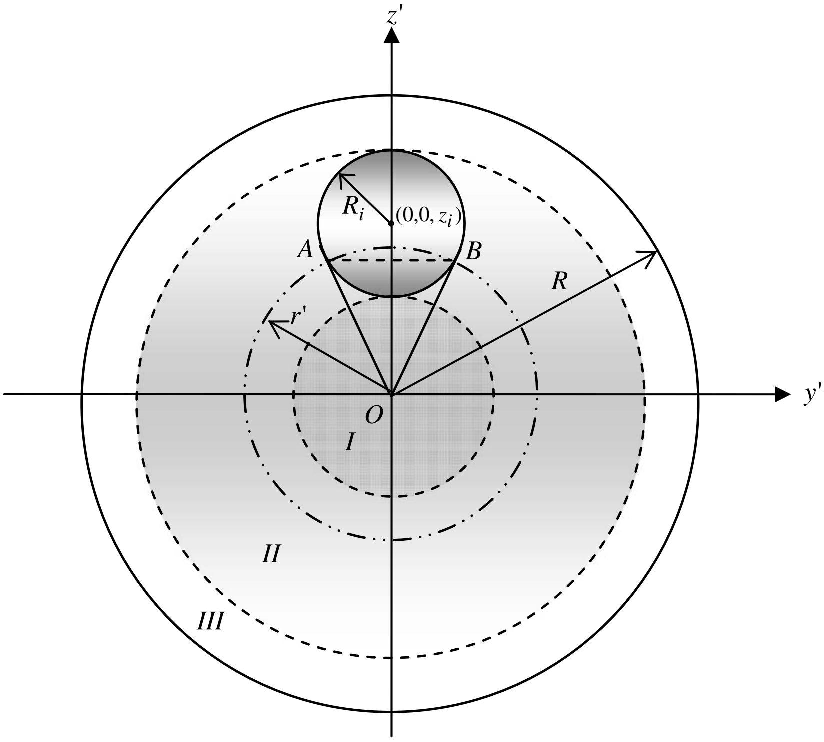

Fig. 1. Computational domains for a spherical source placed on the z-axis.

For a point on the intersection circle of two spheres, polar angle θ' could be related to the other coordinate parameters by

$$\cos\theta' = \frac{z'}{r'} = \frac{z_i^2 - R_i^2 + r'^2}{2z_i r'}. \tag{51}$$

Hence, the differential volume element becomes

$$dV' = r'^2 \sin\theta' d\theta' d\phi' dr' = -r'^2 d(\cos\theta') d\phi' dr', \tag{52}$$

where $\cos\theta'$ is given by (51). This approach could easily be verified simply by evaluating volume of the spherical source with radius R_i centered at $(0,0,z_i)$ as

$$\int_{source} dV' = -\int_{\phi'=0}^{2\pi} \int_{r'=z_i-R_i}^{r'=z_i+R_i} \int_{\cos\theta'=1}^{\frac{z_i^2-R_i^2+r'^2}{2z_i r'}} r'^2 dr' d(\cos\theta') d\phi' = -2\pi \int_{r'=z_i-R_i}^{r'=z_i+R_i} \left(\frac{z_i^2 - R_i^2 + r'^2}{2z_i r'} - 1\right) r'^2 dr' = \frac{4}{3}\pi R_i^3. \tag{53}$$

Using the expressions given by Eqs. (51) and (52) the GF solution could be restated as follows:

$$\begin{aligned} \psi_i(r,\phi,\theta) = {} & \frac{1}{k_{eff}} \int_{r'=r}^{r} \int_{\phi'=0}^{2\pi} \int_{\theta'=0}^{\cos^{-1}\left(\frac{z_i^2-R_i^2+r'^2}{2z_i r'}\right)} \dot{q}_i(r',\phi',\theta') \sum_{\ell=0}^{\infty} \sum_{m=-\ell}^{\ell} g_\ell^2(r,r') Y_\ell^m(\theta,\phi) Y_\ell^{m*}(\theta',\phi') r'^2 \sin\theta' d\theta' d\phi' \\ & + \frac{1}{k_{eff}} \int_{r'=r}^{R} \int_{\phi'=0}^{2\pi} \int_{\theta'=0}^{\cos^{-1}\left(\frac{z_i^2-R_i^2+r'^2}{2z_i r'}\right)} \dot{q}_i(r',\phi',\theta') \sum_{\ell=0}^{\infty} \sum_{m=-\ell}^{\ell} g_\ell^1(r,r') Y_\ell^m(\theta,\phi) Y_\ell^{m*}(\theta',\phi') r'^2 \sin\theta' d\theta' d\phi'. \end{aligned} \tag{54}$$

(1) For a point inside region I, Eq. (54) reads as

$$\psi_i(r,\phi,\theta) = \frac{\dot{q}_i}{k_{eff}} \int_{r'=z_i-R_i}^{r'=z_i+R_i} \int_{\phi'=0}^{2\pi} \int_{\theta'=0}^{\cos^{-1}\left(\frac{z_i^2-R_i^2+r'^2}{2z_i r'}\right)} \sum_{\ell=0}^{\infty} \sum_{m=-\ell}^{\ell} g_\ell^2(r,r') Y_\ell^m(\theta,\phi) Y_\ell^{m*}(\theta',\phi') r'^2 \sin\theta' d\theta' d\phi', \tag{55}$$

or

$$\psi_i(r,\phi,\theta) = \frac{\dot{q}_i}{k_{eff}} \sum_{\ell=0}^{\infty} \int_{r'=z_i-R_i}^{z_i+R_i} r'^2 g_\ell^1(r,r')dr' \int_{\phi'=0}^{2\pi} \int_{\theta'=0}^{\cos^{-1}\left(\frac{z_i^2-R_i^2+r'^2}{2z_ir'}\right)} \sum_{m=-\ell}^{\ell} Y_\ell^m(\theta,\phi)Y_\ell^{m*}(\theta',\phi')\sin\theta' d\theta' d\phi'. \tag{56}$$

Using

$$\int_{\theta'=0}^{\alpha} P_\ell(\cos\theta')\sin\theta' d\theta' = \frac{1}{2\ell+1}[P_{\ell-1}(\cos\alpha) - P_{\ell+1}(\cos\alpha)], \tag{57}$$

and the addition theorem for spherical harmonics

$$\sum_{m=-\ell}^{\ell} Y_\ell^m(\theta,\phi)Y_\ell^{m*}(\theta',\phi') = \frac{2\ell+1}{4\pi}\left\{P_\ell(\cos\theta)P_\ell(\cos\theta') + 2\sum_{m=1}^{\ell}\frac{(\ell-m)!}{(\ell+m)!}P_\ell^m(\cos\theta)P_\ell^m(\cos\theta')\cos m(\phi-\phi')\right\}, \tag{58}$$

excess temperature given by Eq. (56) simplifies to

$$\psi_i(r,\phi,\theta) = \frac{\dot{q}_i}{2k_{eff}} \sum_{\ell=0}^{\infty} P_\ell(\cos\theta)\left[\int_{r'=z_i-R_i}^{z_i+R_i}\left[P_{\ell-1}\left(\frac{z_i^2-R_i^2+r'^2}{2z_ir'}\right) - P_{\ell+1}\left(\frac{z_i^2-R_i^2+r'^2}{2z_ir'}\right)\right]r'^2 g_\ell^2(r,r')dr'\right]. \tag{59}$$

(2) For a point inside region *II*, proceeding in a similar way to (1) results in

$$\begin{aligned}\psi_i(r,\phi,\theta) = {} & \frac{\dot{q}_i}{2k_{eff}} \sum_{\ell=0}^{\infty} P_\ell(\cos\theta)\left[\int_{r'=z_i-R_i}^{r}\left[P_{\ell-1}\left(\frac{z_i^2-R_i^2+r'^2}{2z_ir'}\right) - P_{\ell+1}\left(\frac{z_i^2-R_i^2+r'^2}{2z_ir'}\right)\right]r'^2 g_\ell^2(r,r')dr'\right] \\ & + \frac{\dot{q}_i}{2k_{eff}} \sum_{\ell=0}^{\infty} P_\ell(\cos\theta)\left[\int_{r'=r}^{z_i+R_i}\left[P_{\ell-1}\left(\frac{z_i^2-R_i^2+r'^2}{2z_ir'}\right) - P_{\ell+1}\left(\frac{z_i^2-R_i^2+r'^2}{2z_ir'}\right)\right]r'^2 g_\ell^2(r,r')dr'\right].\end{aligned} \tag{60}$$

(3) For a point inside region *III*, excess temperature is obtained as

$$\psi_i(r,\phi,\theta) = \frac{\dot{q}_i}{2k_{eff}} \sum_{\ell=0}^{\infty} P_\ell(\cos\theta)\left[\int_{r'=z_i-R_i}^{z_i+R_i}\left[P_{\ell-1}\left(\frac{z_i^2-R_i^2+r'^2}{2z_ir'}\right) - P_{\ell+1}\left(\frac{z_i^2-R_i^2+r'^2}{2z_ir'}\right)\right]r'^2 g_\ell^1(r,r')dr'\right]. \tag{61}$$

As a numerical example, temperature field on y–z plane of a pebble is calculated for a spherical source of strength 8.121×10^2 W with a radius of 6.165×10^{-1} cm whose center is placed on the z-axis and 1.5 cm apart from the center of the pebble. Excess temperatures calculated analytically by Eqs. (59)–(61) and by computational fluid dynamics code FLUENT are presented in Table 2.

Series in Eqs. (59)–(61) for three solution domains are truncated when the contribution of the series term begins to cause oscillations in the solution. This is due to the relatively higher frequency oscillations of higher order Legendre polynomials than low order Legendre polynomials. This behavior prevents to calculate the excess temperature to an arbitrary precision. Maximum relative error in excess temperature of analytically obtained results in comparison with FLUENT results is found as 7%. This error falls as much as 1.7% when temperatures are compared instead of excess temperatures. Relative error in excess temperature is about a few percent except for high temperature regions, that is the neighborhood of the spherical source.

4.3. An arbitrarily located spherical source

In this most general case, a spherical source of radius R_i with a uniform volumetric heat generation rate $\dot{q}_i$ is located at a position $\mathbf{r_i} = (r_i, \phi_i, \theta_i)$ in polar spherical coordinates system or (x_i, y_i, z_i) in Cartesian coordinate system, within the graphite sphere of radius R. The solution obtained in the previous part for a source located on a specified axis allows one to calculate temperature distribution for an arbitrarily located source by using orthogonal coordinate transformations (Fig. 2).

The strategy is to fit the position vector $\mathbf{r_i}$ of the center of the spherical source with the z-axis of the final coordinate system. This is accomplished rotating our physical coordinate system (x,y,z) first about z-axis by an angle α, and then rotating new coordinate system denoted by (x_1, y_1, z_1) about y_1-axis by an angle β to get final coordinate system denoted by (x,y,z). Since the length of vectors is invariant under orthogonal transformations, these Euler angles will be $\alpha = \phi_i$ and $\beta = \theta_i$, where θ_i and ϕ_i are polar and azimuth angles of the position of the center of the spherical source, respectively.

Rotation matrices about z and y_1 axis denoted by $\mathbf{R_z}$ and $\mathbf{R}_y$ are given as

$$\mathbf{R_z} = \begin{bmatrix} \cos\varphi_i & \sin\varphi_i & 0 \\ -\sin\varphi_i & \cos\varphi_i & 0 \\ 0 & 0 & 1 \end{bmatrix}, \quad \mathbf{R_y} = \begin{bmatrix} \cos\theta_i & 0 & -\sin\theta_i \\ 0 & 1 & 0 \\ \sin\theta_i & 0 & \cos\theta_i \end{bmatrix}. \tag{62}$$

Table 2
Excess temperatures on the y–z plane calculated analytically and by FLUENT for a spherical source located at $(x,y,z) = (0,0,1.5)$.

r	θ											
	0	$\pi/10$	$2\pi/10$	$3\pi/10$	$4\pi/10$	$5\pi/10$	$6\pi/10$	$7\pi/10$	$8\pi/10$	$9\pi/10$	π	
0.0	75.48	75.48	75.48	75.48	75.48	75.48	75.48	75.48	75.48	75.48	75.48	*Fluent*
	74.64	74.64	74.64	74.64	74.64	74.64	74.64	74.64	74.64	74.64	74.64	Analytic
0.3	106.79	104.72	98.75	91.32	82.66	73.57	67.74	62.17	59.85	57.63	56.35	*Fluent*
	102.19	100.11	94.57	87.17	79.45	72.44	66.61	62.13	58.99	57.14	56.52	Analytic
0.6	145.71	137.67	118.33	101.19	82.94	66.67	55.64	50.44	46.39	43.60	42.17	*Fluent*
	148.64	139.21	117.90	97.22	79.08	66.90	56.97	51.34	46.86	44.55	43.80	Analytic
0.9	226.33	196.69	140.07	105.51	78.53	60.19	47.92	40.22	35.60	33.00	32.21	*Fluent*
	242.18	201.43	141.07	99.98	79.50	59.63	48.19	41.55	37.41	30.74	34.42	Analytic
1.2	319.59	259.78	154.22	97.18	68.19	49.52	40.10	31.99	27.85	26.64	26.26	*Fluent*
	338.53	274.99	151.34	93.32	66.92	50.68	39.54	33.70	29.80	27.00	27.63	Analytic
1.5	350.85	274.55	145.00	84.15	56.02	38.80	31.13	26.30	23.78	21.34	20.53	*Fluent*
	364.42	273.89	142.01	83.80	56.59	40.35	32.81	27.24	24.00	22.40	20.85	Analytic
1.8	320.98	229.09	117.56	71.88	45.95	32.99	25.31	21.31	19.17	17.70	16.85	*Fluent*
	330.55	228.86	117.30	69.96	45.95	33.94	26.38	21.82	19.12	17.65	17.06	Analytic
2.1	229.02	166.19	96.58	58.84	38.68	25.41	20.64	16.97	14.88	14.26	13.43	*Fluent*
	239.17	164.16	97.83	57.01	38.78	27.12	21.12	17.01	15.17	13.97	13.53	Analytic
2.4	150.88	123.61	75.97	45.11	29.36	21.26	16.77	13.28	11.37	10.78	10.38	*Fluent*
	144.85	113.52	70.95	44.67	30.03	21.62	16.60	13.66	11.87	10.94	10.71	Analytic
2.7	104.12	88.40	53.69	33.84	22.66	17.03	12.97	10.38	8.84	8.19	8.00	*Fluent*
	97.59	80.73	53.46	34.39	23.19	16.67	12.80	10.49	9.11	8.39	8.16	Analytic
3.0	75.83	64.02	39.20	25.93	17.64	12.87	9.76	7.98	6.84	6.38	6.21	*Fluent*
	69.64	58.54	39.52	25.62	17.29	12.43	9.54	7.81	6.78	6.24	6.14	Analytic

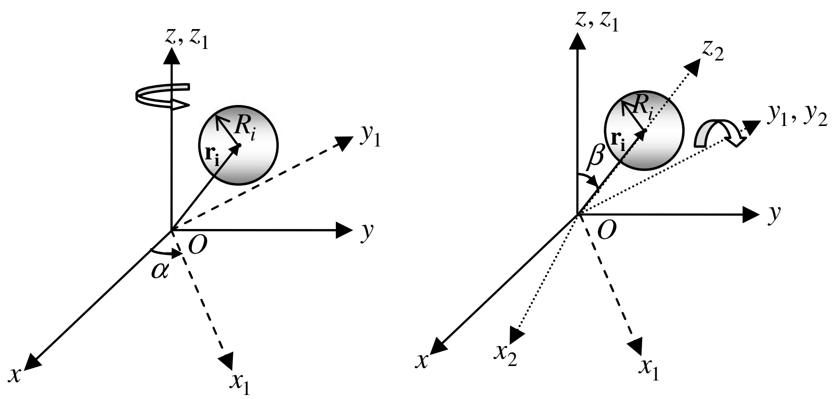

Fig. 2. Coordinate transformation for an arbitrarily placed spherical source.

The rotation matrix for these two successive rotations is

$$\mathbf{R}_y\mathbf{R}_\mathbf{z} = \mathbf{R}_{yz} = \begin{bmatrix} \cos\theta_i\cos\phi_i & \cos\theta_i\sin\phi_i & -\sin\phi_i \\ -\sin\phi_i & \cos\phi_i & 0 \\ \sin\theta_i\cos\phi_i & \sin\theta_i\sin\phi_i & \cos\theta_i \end{bmatrix}. \tag{63}$$

The physical domain (x,y,z) is related to the computational domain (x_2,y_2,z_2) as follows:

$$\begin{bmatrix} x_2 \\ y_2 \\ z_2 \end{bmatrix} = \begin{bmatrix} \cos\theta_i\cos\phi_i & \cos\theta_i\sin\phi_i & -\sin\phi_i \\ -\sin\phi_i & \cos\phi_i & 0 \\ \sin\theta_i\cos\phi_i & \sin\theta_i\sin\phi_i & \cos\theta_i \end{bmatrix} \begin{bmatrix} x \\ y \\ z \end{bmatrix}. \tag{64}$$

For a point $(x,y,z) = (r\sin\theta\cos\phi, r\sin\theta\sin\phi, r\cos\theta)$ in our physical domain, this point's correspondence in the computational domain (x_2,y_2,z_2) could be calculated using Eq. (64). Since the spherical source is located on the z_2-axis of the computational domain, azimuthally symmetric case solutions given by Eqs. (59)–(61) apply with the modification that θ is replaced by $\theta_2 = \cos^{-1}(z_2/r)$.

The outlined procedure is applied to calculate excess temperature field on the y–z plane for a spherical source of strength 812.1 W with a radius of 6.165×10^{-1} cm whose center is placed at $\mathbf{r}_i = (2, \pi/4, 3\pi/4)$ in spherical coordinates. Calculated results are given in Table 3 together with the results of FLUENT. Maximum relative error in excess temperature of analytically

Table 3
Excess temperatures on the y–z plane calculated analytically and by FLUENT for a spherical source located at $(r_i, \phi_i, \theta_i) = (2, \pi/4, 3\pi/4)$.

ϕ	$\pi/2$						$3\pi/2$				
r	θ						θ				
	0	$2\pi/10$	$4\pi/10$	$6\pi/10$	$8\pi/10$	π	$8\pi/10$	$6\pi/10$	$4\pi/10$	$2\pi/10$	
0.0	44.79	44.79	44.79	44.79	44.79	44.79	44.79	44.79	44.79	44.79	*Fluent*
	46.29	46.29	46.29	46.29	46.29	46.29	46.29	46.29	46.29	46.29	Analytic
0.3	37.28	41.11	46.90	52.67	55.85	53.24	47.11	41.20	37.33	36.28	*Fluent*
	38.53	42.41	48.45	54.76	57.71	54.97	48.72	42.62	38.64	37.26	Analytic
0.6	30.89	36.75	47.33	61.12	69.14	61.99	47.35	36.82	31.28	29.41	*Fluent*
	31.84	37.71	48.63	63.39	72.01	63.97	49.18	38.05	32.00	30.08	Analytic
0.9	25.59	31.69	45.20	68.33	86.39	69.14	45.99	32.24	25.73	23.81	*Fluent*
	26.18	32.73	46.74	70.89	89.22	72.00	47.53	33.13	26.35	24.33	Analytic
1.2	20.93	27.22	41.69	72.40	102.10	75.15	42.76	27.78	21.10	19.44	*Fluent*
	21.43	27.87	43.12	75.36	107.70	77.09	44.04	28.28	21.58	19.68	Analytic
1.5	17.11	22.63	37.29	72.44	117.83	74.89	38.19	23.21	17.29	15.60	*Fluent*
	17.43	23.33	38.36	75.06	122.23	77.25	39.33	23.69	17.59	15.93	Analytic
1.8	13.93	18.82	32.35	67.17	119.97	70.27	33.18	19.14	14.03	12.59	*Fluent*
	14.09	19.18	33.21	69.51	124.46	71.91	34.14	19.44	14.28	12.99	Analytic
2.1	11.20	15.29	26.98	59.44	109.74	61.61	27.85	15.69	11.33	10.08	*Fluent*
	11.26	15.52	27.82	60.67	113.27	62.90	28.65	15.71	11.45	10.45	Analytic
2.4	8.84	12.32	21.96	49.83	92.71	52.11	22.55	12.52	8.93	8.00	*Fluent*
	8.85	12.38	22.32	50.82	94.86	52.67	23.02	12.59	8.95	8.04	Analytic
2.7	6.93	9.61	17.29	39.88	72.32	41.03	17.87	9.86	6.91	6.19	*Fluent*
	6.82	9.59	17.38	40.45	74.27	41.95	17.91	9.79	6.87	6.09	Analytic
3.0	5.21	7.28	13.19	30.40	54.97	31.57	13.64	7.47	5.26	4.68	*Fluent*
	5.08	7.16	13.04	30.39	55.46	31.52	13.44	7.30	5.12	4.55	Analytic

obtained results in comparison with FLUENT results is found as 5.48%. This error falls as much as 0.69% when temperatures are compared instead of excess temperatures.

4.4. Two spherical sources

This case provides no further qualitative knowledge than the previous case in which a single arbitrarily placed source is studied except that whether truncating errors phase out by using superposition principle. Calculations are carried out for two spherical sources and resulting excess temperatures are compared with the FLUENT results. Each sources are of with a strength of 406.061 W with radius 0.489 cm and located at the positions $(x_1, y_1, z_1) = (0, 0, 1.5)$ and $(r_2, \phi_2, \theta_2) = (2, \pi/4, 3\pi/4)$, respectively. Calculated results are given in Table 4 with results of FLUENT.

In this case study, maximum relative error of analytically obtained results in comparison with FLUENT results is found as 6.67%. This error falls as much as 1.49% when temperatures are compared instead of excess temperatures. It is observed that truncating errors arising from series solution for each source are not magnified when principle of superposition is used.

4.5. Three spherical sources

When the kernels have relatively too small dimensions in comparison with the pebble, negligibility of volumetric effects could be investigated by taking kernels as point sources in analytical solution. In the FLUENT runs, heat generating kernels within the pebble is represented by three spherical sources each has volumes with one-third of the total volume of kernels. These three sources are assumed to be point sources in the analytical GF solution. Results of two calculations are compared to assess the validity of point source approximation.

A point source located at $\mathbf{r_i} = (r_i, \varphi_i, \theta_i)$ with strength q_i could be represented in the computational or primed coordinate system as

$$\dot{q}_i(r', \varphi\prime, \theta') = q_i \delta(\mathbf{r}' - \mathbf{r_i}) = q_i \frac{\delta(r' - r_i)\delta(\theta' - \theta_i)\delta(\varphi' - \varphi_i)}{r'^2 \sin\theta'}. \quad (65)$$

Introducing Eqs. (65) and (17) into Eq. (15), excess temperature is obtained as follows:

$$\psi_i(r, \varphi, \theta) = \frac{q_i}{k_{eff}} \int_{r'} \int_{\varphi\prime} \int_{\theta'} \sum_{\ell=0}^{\infty} \sum_{m=-\ell}^{\ell} \delta(r' - r_i)\delta(\theta' - \theta_i)\delta(\varphi' - \varphi_i) g_\ell(r', r) Y_\ell^m(\theta', \varphi') Y_\ell^{m*}(\theta, \varphi) d\theta' d\varphi' dr'. \quad (66)$$

Above expression is simplified using sifting property of Dirac's delta function as

$$\psi_i(r, \phi, \theta) = \frac{q_i}{k_{eff}} \sum_{\ell=0}^{\infty} g_\ell(r_i, r) \sum_{m=-\ell}^{\ell} Y_\ell^m(\theta, \phi) Y_\ell^{m*}(\theta, \phi). \quad (67)$$

Table 4
Excess temperatures on the y–z plane calculated analytically and by FLUENT for two spherical sources located at $(x_1, y_1, z_1) = (0, 0, 1.5)$ and $(r_2, \phi_2, \theta_2) = (2, \pi/4, 3\pi/4)$.

ϕ	$\pi/2$						$3\pi/2$				
r	θ						θ				
	0	$2\pi/10$	$4\pi/10$	$6\pi/10$	$8\pi/10$	π	$8\pi/10$	$6\pi/10$	$4\pi/10$	$2\pi/10$	
0.0	58.42	58.42	58.42	58.42	58.42	58.42	58.42	58.42	58.42	58.42	*Fluent*
	60.46	60.46	60.46	60.46	60.46	60.46	60.46	60.46	60.46	60.46	Analytic
0.3	67.43	65.93	61.65	58.43	56.45	53.90	52.15	52.60	57.11	63.45	*Fluent*
	70.36	68.49	63.95	60.68	58.35	55.75	53.85	54.62	59.05	65.91	Analytic
0.6	86.97	74.81	61.81	58.26	57.35	52.22	46.38	45.93	53.89	71.18	*Fluent*
	90.24	78.01	64.04	60.36	59.44	53.89	48.02	47.69	55.72	74.19	Analytic
0.9	126.71	83.26	58.43	57.52	61.40	51.42	41.22	39.37	48.72	79.31	*Fluent*
	132.55	86.90	60.64	59.54	63.32	53.22	42.53	41.08	50.05	83.09	Analytic
1.2	202.44	86.27	52.79	55.67	65.76	50.87	35.97	33.08	42.41	82.23	*Fluent*
	215.28	89.84	54.66	57.59	68.78	52.02	36.96	34.05	43.90	85.75	Analytic
1.5	232.53	78.44	46.03	52.25	70.71	48.10	30.82	27.35	35.80	74.90	*Fluent*
	245.54	82.96	47.46	53.87	73.08	50.76	31.63	28.17	37.03	78.88	Analytic
1.8	202.14	65.84	39.07	46.59	69.57	43.64	25.98	22.44	29.56	62.36	*Fluent*
	215.62	63.06	39.96	48.23	72.48	44.48	26.96	22.99	30.53	65.50	Analytic
2.1	120.79	52.03	32.04	40.18	62.52	37.55	21.43	18.15	24.15	49.88	*Fluent*
	125.45	54.08	32.53	41.32	65.11	38.58	21.60	18.53	24.70	51.46	Analytic
2.4	73.62	40.24	25.76	33.21	52.39	31.43	17.15	14.43	19.16	38.54	*Fluent*
	76.76	41.70	26.24	33.74	53.25	31.76	17.51	14.63	19.38	39.35	Analytic
2.7	51.20	30.92	20.13	26.41	40.83	24.63	13.51	11.31	14.85	29.18	*Fluent*
	51.25	33.29	20.31	26.59	41.69	25.03	12.83	11.29	15.02	31.13	Analytic
3.0	36.86	23.21	15.28	20.08	31.02	18.91	10.28	8.57	11.31	21.95	*Fluent*
	38.46	23.25	15.04	19.80	30.94	18.64	10.01	8.30	11.06	21.90	Analytic

Using addition theorem of spherical harmonics stated in Eqs. (58) and (67) becomes

$$\psi_i(r,\phi,\theta) = \frac{q_i}{k_{eff}} \sum_{\ell=0}^{\infty} g_\ell(r_i, r) \frac{2\ell+1}{4\pi} \left[P_\ell(\cos\theta) P_\ell(\cos\theta_i) + 2 \sum_{m=1}^{\ell} \frac{(\ell-m)!}{(\ell+m)!} P_\ell^m(\cos\theta) P_\ell^m(\cos\theta_i) \cos m(\phi - \phi_i) \right]. \tag{68}$$

Table 5
Excess temperatures on the y–z plane calculated with point source approximation and by FLUENT for three spherical sources located at $(x_1, y_1, z_1) = (0, 0, 1.5)$, $(r_2, \phi_2, \theta_2) = (2, \pi/4, 3\pi/4)$ and $(r_3, \phi_3, \theta_3) = (2.5, 5\pi/4, 3\pi/4)$.

ϕ	$\pi/2$						$3\pi/2$				
r	θ						θ				
	0	$2\pi/10$	$4\pi/10$	$6\pi/10$	$8\pi/10$	π	$8\pi/10$	$6\pi/10$	$4\pi/10$	$2\pi/10$	
0.0	48.54	48.54	48.54	48.54	48.54	48.54	48.54	48.54	48.54	48.54	*Fluent*
	50.07	50.07	50.07	50.07	50.07	50.07	50.07	50.07	50.07	50.07	Analytic
0.3	53.15	51.83	49.26	47.94	47.69	47.16	46.46	46.30	48.07	51.22	*Fluent*
	55.14	53.63	50.89	49.52	49.16	48.61	47.86	47.82	49.57	52.96	Analytic
0.6	64.82	56.35	48.12	46.96	48.55	47.75	45.30	43.52	46.11	55.53	*Fluent*
	67.04	58.51	49.61	48.43	50.06	49.14	46.64	44.91	47.47	57.58	Analytic
0.9	90.16	60.80	44.70	45.56	51.06	48.90	44.74	40.60	42.45	60.05	*Fluent*
	95.18	63.25	46.19	46.93	52.45	50.39	46.13	41.83	43.71	62.27	Analytic
1.2	151.65	61.87	39.99	43.41	53.54	49.77	44.81	37.77	37.69	61.10	*Fluent*
	186.44	64.13	41.21	44.67	55.59	51.12	46.11	38.72	38.78	63.23	Analytic
1.5	181.79	55.82	34.64	40.23	56.03	48.82	45.00	34.52	32.47	55.31	*Fluent*
	–	56.70	36.99	43.86	60.77	68.77	49.41	38.05	35.16	55.92	Analytic
1.8	151.63	46.77	29.30	35.58	54.37	45.71	44.98	30.91	27.28	46.03	*Fluent*
	182.69	48.56	29.78	36.63	56.13	46.90	45.93	31.76	27.98	47.91	Analytic
2.1	83.71	37.00	23.97	30.53	48.55	40.69	43.21	27.24	22.56	36.89	*Fluent*
	86.58	38.28	24.53	31.56	51.09	41.63	44.31	27.41	23.12	37.74	Analytic
2.4	51.27	28.67	19.25	25.17	40.60	34.84	38.71	22.96	18.09	28.63	*Fluent*
	53.63	29.46	19.69	25.13	41.55	35.15	40.98	23.71	18.52	29.06	Analytic
2.7	35.82	22.04	15.03	20.00	31.80	27.96	32.51	18.60	14.15	21.75	*Fluent*
	36.45	22.38	15.14	19.92	32.24	28.22	33.35	18.68	14.28	22.06	Analytic
3.0	25.83	16.56	11.41	15.20	24.16	21.53	25.40	14.23	10.79	16.37	*Fluent*
	26.08	16.59	11.28	15.00	24.04	21.33	25.31	14.03	10.64	16.35	Analytic

Excess temperature for three point sources could be calculated using principle of superposition which reads as

$$\psi(r,\varphi,\theta) = \sum_{i=1}^{3} \psi_i(r,\varphi,\theta), \tag{69}$$

where $\psi_i(r,\varphi,\theta)$ is calculated according to (68).

Numerical example of this part considers three equal volumes of spherical sources each with source strength of 270.707 W which is one-third of pebble heat generating rate. Radii of these sources are 0.427 cm and positions of their centers are chosen as $(x_1,y_1,z_1) = (0,0,1.5)$, $(r_2,\phi_2,\theta_2) = (2,\pi/4,3\pi/4)$, and $(r_3,\phi_3,\theta_3) = (2.5,5\pi/4,3\pi/4)$.

Table 5 shows results of analytical computations with point source approximation and FLUENT results for spherical sources having the same strengths with the point sources. An increased maximum relative error of 22.94% in excess temperature is observed around the center of the spherical source as expected due to point source approximation in our analytical solution. This error falls as much as 4.08%, if temperatures are compared. Another disadvantage of the point source approximation is the failure to calculate the excess temperature at the center of the spherical sources as seen from the Table 5. Except for the closed periphery of the point sources a faster convergency and better accuracy is achieved in the point source approximation. It is clear that point source approximation would provide a more effective analytical solution with acceptably small relative error for 15,000 kernels (approximate actual number of fuel kernels in a pebble) each with a diameter of 0.5 mm which is two small in comparison with the dimensions used (42.7 mm) in this part of the calculations.

5. Conclusions

Green's function solution of heat diffusion equation for a finite sphere cooled convectively and containing arbitrarily placed spherical sources is obtained in this study. Spherical harmonics expansion is employed to find the GF of heat diffusion operator with Robin (mixed) boundary condition. Analytical solution to this seemingly simple problem has been observed to be associated with some numerical convergency problems resulting from high-frequency oscillatory behavior of Legendre polynomials at high order. It is further demonstrated that analytical solution to the diffusion equation in a sphere having spherical sources inside could be reduced to a more simple form with point source approximation when the dimensions of the sources are relatively small in comparison with the pebble, which is the case for pebble bed reactors.

Even though analytical treatment seems feasible it is concluded that examining the stochastic effect of distribution of thousands tiny fuel kernels inside the pebbles of a pebble bed reactors dictates much better convergency to eliminate overlapping of truncation error and small contribution of each kernel to the temperature field. The analytical solution derived in this work could be used as a verification tool of the CFD codes to some extent.

Acknowledgements

Author would like to expresses special thanks to Mehmet Tombakoglu of Nuclear Engineering Department of Hacettepe University and Muhammet Barik of Turkish Atomic Energy Authority for their valuable suggestions and help.

References

[1] K.D. Cole, D.H.Y. Yen, Green's functions, temperature and heat flux in the rectangle, Int. J. Heat Mass Transfer 44 (2001) 3883–3894.
[2] P.M. Morse, H. Feshbach, Methods of Theoretical Physics, McGraw-Hill, New York, 1953.
[3] H.S. Carslaw, J.C. Jaeger, Conduction of Heat in Solids, Oxford University Press, Oxford, 1959.
[4] I. Stakgold, Boundary Value Problems of Mathematical Physics, Macmillan, New York, 1967.
[5] G. Barton, Elements of Green's Functions and Propagation, Oxford University Press, Oxford, 1989.
[6] A.G. Butkovskii, Green's Functions and Transfer Functions Handbook, Halsted Press (division of Wiley), New York, 1992.
[7] A.G. Butkovskii, L.M. Pustyl'nikov, Characteristics of Distributed-Parameter Systems, Kluwer Academic Publishers., Dorddrecht, 1993.
[8] J.V. Beck, K.D. Cole, A. Haji-Sheikh, B. Litkouhi, Heat Conduction Using Green's Function, Hemisphere, New York, 1992.
[9] I.M. Dolgova, Y.A. Melnikov, Construction of Green's functions and matrices for equations and systems of the elliptic type, J. Appl. Math. Mech. 42 (1978) 740–746.
[10] Y.A. Melnikov, Green's Functions in Applied Mechanics, Computational Mechanics Publications, Boston, 1995.
[11] Y.A. Melnikov, Influence Functions and Matrices, Marcel Dekker, New York, 1999.
[12] K.D. Cole, H.K. Kim, Green's functions for steady two-dimension heat conduction, in: Proceedings of the 10th International Heat Transfer Conference, Brighton, UK, vol. 6, 1994, pp. 331–336.
[13] K.N. Theologos, I.D. Nikou, A.I. Lygeros, N.C. Markatos, Simulation and design of fluid catalytic-cracking riser-type reactors, AIChE J. 43 (1997) 486–494.
[14] N.V. Dewachtere, G.F. Froment, I. Vasalos, N. Markotos, N. Skandalis, Advanced modeling of riser-type catalytic-cracking reactors, Appl. Therm. Eng. 17 (1997) 837–844.
[15] N.C. Markatos, Modelling of two-phase transient flow and combustion of granular propellants, Int. J. Multiphase Flow 12 (1986) 913–933.
[16] PBMR Ltd., Reactor safety analysis report of the South-African pebble bed modular reactor (PBMR), Rev. E, 2000, Centurion, South Africa.
[17] H.D. Gougar, Advanced core design and fuel management for pebble-bed reactors, Ph.D. Dissertation, The Graduate School, Department of Mechanical and Nuclear Engineering, The Pennsylvania State University, 1983.
[18] B.R. Bird, W.E. Stewart, E.N. Lightfood, Transport Phenomena, second ed., Wiley, New York, 2001 (Chapter 9.6).
[19] G.B. Arfken, H.J. Weber, Mathematical Methods for Physicists, fivth ed., Academic Press, London, 2001 (Chapter 8.7).
[20] V. Gnielinski, Gleichungen zur Berechnung des wärme- und stoffaustausches in durchströmten ruhenden kugelschütten bei mittleren und großen Peclet-Zahlen, Verfahrenstechnik 12 (6) (1978) 363–366.
[21] Y. Sun, Z.Gao, Evaluation of high temperature gas cooled reactor performance, prepared for the IAEA coordinated research program (CRP-5), Institute of Nuclear Energy Technology, Beijing 100084, PR China, December 2003.